

A Globally Accelerated Numerical Method For Optical Tomography With Continuous Wave Source

Hua Shan[▽], Michael V. Klibanov^{*}, Jianzhong Su[▽], Natee Pantong[▽], and Hanli Liu[▷]

[▽]Department of Mathematics
University of Texas at Arlington
Arlington, TX 76019

^{*}Department of Mathematics and Statistics
University of North Carolina at Charlotte,
Charlotte, NC 28223

[▷] Department of Bioengineering
University of Texas at Arlington
Arlington, TX 76019
E-mail: mklibanv@uncc.edu

May 29, 2018

Abstract

A new numerical method for an inverse problem for an elliptic equation with unknown potential is proposed. In this problem the point source is running along a straight line and the source-dependent Dirichlet boundary condition is measured as the data for the inverse problem. A rigorous convergence analysis shows that this method converges globally, provided that the so-called tail function is approximated well. This approximation is verified in numerical experiments, so as the global convergence. Applications to medical imaging, imaging of targets on battlefields and to electrical impedance tomography are discussed.

1 Introduction

The phenomenon of multiple local minima and ravines of least squares residual functionals represents the major obstacle for reliable numerical solutions of Multidimensional Coefficient Inverse Problems (MCIPs) for Partial Differential Equations (PDEs). We believe that because of the applied nature of the discipline of Inverse Problems, the issue of addressing the problem of local minima has *vital importance* for this discipline. Indeed, any gradient-like

optimization method for such a functional would likely converge to a local minimum, which is located far from the correct solution. Furthermore, a global minimum, even a well pronounced one, is not necessarily located close to the true solution, because of the ill-posed nature of MCIPs. Because of this, the vast majority of current numerical methods for MCIPs are locally convergent ones, like, for example Newton-like method, see, e.g., [1],[2],[4],[5] and many issues of Inverse Problems. That is, convergence of such a method to the true solution is rigorously guaranteed only if the initial guess is located sufficiently close to that solution. However, in the majority of applications such as e.g., medical and military ones, the media of interest is highly heterogeneous, which means that a good first guess is unknown. The latter naturally raises the question about the reliability of locally convergent numerical methods for those applications, and this question is well known to many practitioners working on computations of real world MCIPs.

Thus, we are interested in the issue of globally convergent numerical methods for MCIPs. We call a numerical method *globally convergent* if the following two conditions are in place: (1) a rigorous convergence analysis ensures that this method leads to a good approximation of the true solution *regardless* on the availability of a first good guess, and (2) numerical experiments confirm the said convergence property.

In this paper we present an “almost” globally convergent method for an MCIP for the equation

$$\Delta_{\mathbf{x}}u - a(\mathbf{x})u = -\delta(\mathbf{x} - \mathbf{x}_0), \mathbf{x} = (x, z) \in \mathbb{R}^2, \quad (1.1)$$

$$\lim_{|\mathbf{x}| \rightarrow \infty} u(\mathbf{x}, \mathbf{x}_0) = 0. \quad (1.2)$$

Here \mathbf{x}_0 is the source position, and this position is running along a line to generate the data for the inverse problem. We use the word “almost”, because we rigorously prove global convergence only assuming that we know a good approximation for the so-called “tail function”, i.e., we assume that we know a good approximation of the second term of the asymptotic behavior of the function $\ln[u(\mathbf{x}, \mathbf{x}_0)]$ for $|\mathbf{x}_0| \rightarrow \infty$. Since this approximation is unknown analytically, we have decided to use a heuristic iterative “accelerator” for convergence of tails and to confirm the desired convergence numerically. Assuming that our tail function is close to the correct one, we prove a global convergence result, which does not rely on a good first guess for the solution. This is why we call our method “globally accelerated”. From the numerical standpoint, another advantage for using the accelerator is that it gives us an approximation for the tail, which seems to be rather close to the actual tail and we observe this numerically. The only drawback is that we cannot establish this rigorously.

We assume throughout this paper that the function $a \in C^\alpha(\mathbb{R}^2)$, $a \geq \text{const.} > 0$ and $a(\mathbf{x}) = k^2 = \text{const.} > 0$ for $\mathbf{x} \in \mathbb{R}^2 \setminus \Omega$, where $\alpha \in (0, 1)$. The classic theory implies that there exists unique solution of the problem (1.1), (1.2) such that $u \in C^{2+\alpha}(|\mathbf{x} - \mathbf{x}_0| \geq \epsilon)$, $\forall \epsilon > 0$.

The first generation of globally convergent numerical methods has started from the so-called convexification algorithm [6]. The convexification is using the projection technique with respect to all variables, except of one, and a stable layer stripping procedure with respect to the latter variable. While the work [6] is concerned with time/frequency dependent data, our publication [8] is applying the convexification to the case of the running source,

which is the same as one in this paper. In the mathematics literature some other numerical techniques providing the global convergence (see, e.g., [15-20]) are available. Their numerical implementations can be found in [21-24].

Recently the development of the second generation of globally convergent numerical methods was initiated in [3]. The idea of [3] was originated from our earlier publication [9]. The concept of [3] also overlaps in part with the scheme of the current paper. However, unlike our current case, the time dependent data resulted from a single measurement are considered in [3]. Laplace transform of either hyperbolic or parabolic equation of [3] leads to the equation $\Delta w - s^2 c(\mathbf{x})w - a(\mathbf{x})w = -\delta(\mathbf{x} - \mathbf{x}_0)$, where $s > 0$ is the parameter of the Laplace transform and the source position is fixed. Compared with our case, the main advantage of this equation is that the asymptotic behavior of tails at $s \rightarrow \infty$ is known. Specifically, in the case when the coefficient $c(\mathbf{x})$ is unknown, $\lim_{s \rightarrow \infty} (\ln w/s^2) = 0$, and similarly when $a(x)$ is unknown. Ultimately, the knowledge of these limits enables one to prove a global convergence theorem in [3] without a heuristic assumption.

We are interested in the extension of the idea of [3] to the case of the running source instead of the changing time or frequency. In other words, we consider almost the same inverse problem as one in [8]. However, instead of the convexification of [8] we develop an analogue of the method [3]. A numerical method, similar with one of this publication, was published in our early work [9]. However, the treatment of tails in section 4 of [9] was different from one of our case, and that is why the global convergence property was not observed in [9]. We also refer to subsection 5.4 of [4] for another treatment of tails for a Newton-like locally convergent method for an MCIP with frequency dependent data. We now explain the underlying reason of our difficulties with the tail function from the physics standpoint. In the case of the time dependent data for a hyperbolic equation [3] the tail function is close to the so-called “first arrival wave”. It is well known that the first arrival signal is very informative one. However, it is unclear what the first arrival signal is in our case of the elliptic equation (1.1) with the running source.

We now formulate our inverse problem.

Inverse Problem. Denote $\mathbf{x} = (x, z)$. Let $\Omega \subset \mathbb{R}^2$ be a bounded domain and $\Gamma = \partial\Omega$. Let B be a constant. Suppose that in (1.1) $\mathbf{x}_0 = (s, B) \notin \overline{\Omega}$. Determine the coefficient $a(x)$ for $x \in \Omega$, assuming that the following function $\varphi(\mathbf{x}, s)$ is given

$$u(\mathbf{x}, s) = \varphi(\mathbf{x}, s), \forall \mathbf{x} \in \Gamma, \forall s \in [\underline{s}, \bar{s}], \quad (1.3)$$

where \bar{s} is a sufficiently large number, $\underline{s} < \bar{s}$ is a certain fixed number and $\{\mathbf{x} = (s, B), s \geq \underline{s}\} \cap \partial\Omega = \emptyset$.

We consider the 2-D case for the sake of simplicity only for this complicated problem. Generalizations of our method on the 3-D case are feasible. The parameter count shows that the data $\varphi(\mathbf{x}, s)$ depends on two free parameters, so as the unknown coefficient $a(\mathbf{x})$. Hence, this Inverse Problem is non-overdetermined. This inverse problem has applications in imaging using light propagation in a diffuse medium. This is the so-called continuous-wave (CW) light. In this case the coefficient $a(\mathbf{x})$ is

$$a(\mathbf{x}) = 3(\mu'_s \mu_a)(\mathbf{x}), \quad (1.4)$$

where $\mu'_s(\mathbf{x})$ is the reduced scattering coefficient and $\mu_a(\mathbf{x})$ is the absorption coefficient of the medium [1]. The first example of this application is imaging of targets on battlefields covered by smog and flames using propagation of light originated by lasers. In this application the laser source should be moved along a line and the measurements of the output light should be performed at the boundary of the domain of interest. Interestingly, the diffuse-like propagation of light would be even helpful, because the direct light can miss the target. The second applied example is in imaging of human organs or small animals using near infrared light propagation. Note that this application is discussed in many publications, in which locally convergent numerical methods are developed, see, e.g., [1],[9],[13]. Also, the above Inverse Problem has applications in Electrical Impedance Tomography, in which case the original equation is $\nabla \cdot (\sigma(\mathbf{x}) \nabla v) = -\delta(\mathbf{x} - \mathbf{x}_0)$ and the standard change of variables $u = v\sqrt{\sigma}$ reduces this equation to (1.1) assuming that $\sigma(\mathbf{x}) = 1$ in a neighborhood of the source position \mathbf{x}_0 . Here $\sigma(\mathbf{x}) \geq \text{const.} > 0$ is the electric conductivity of the medium.

2 Nonlinear Integral Differential Equation

Since the function u is positive, the by the maximum principle we can consider the function $v = \ln u$. Since the source $\mathbf{x}_0 = (s, B) \notin \Omega$, we obtain the following equation from (1.1)

$$\Delta v + |\nabla v|^2 = a(\mathbf{x}) \quad \text{in } \Omega, \quad (2.1)$$

$$v(\mathbf{x}, s) = \varphi_1(\mathbf{x}, s), \quad \forall (\mathbf{x}, s) \in \Gamma \times (A, \bar{s}), \quad (2.2)$$

where $\varphi_1 = \ln \varphi$. To eliminate the unknown coefficient $a(\mathbf{x})$ from equation (2.1), differentiate it with respect to s and let

$$q(\mathbf{x}, s) = \partial_s v(\mathbf{x}, s). \quad (2.3)$$

Then

$$v(\mathbf{x}, s) = - \int_s^{\bar{s}} q(\mathbf{x}, \tau) d\tau + T(\mathbf{x}), \quad \mathbf{x} \in \Omega, s \in (\underline{s}, \bar{s}] \quad (2.4)$$

In (2.4) $T(\mathbf{x})$ is the so-called ‘‘tail function’’. The exact expression for this function is of course $T(\mathbf{x}) = v(\mathbf{x}, \bar{s})$. We know only the first term of the asymptotic expansion of the function $v(\mathbf{x}, \bar{s})$ at $\bar{s} \rightarrow \infty$ (below). As it was pointed out in Introduction, if we would know the second term also, as it is the case of the time dependent data of [3], then we would be better off approximating the tail function. However, the absence of the knowledge of this term significantly complicates the matter compared with [3]. Thus, we develop below a heuristic iterative procedure of an iterative approximation of the function $T(\mathbf{x})$, with the aim of finding such an approximation $T_{appr}(\mathbf{x})$ that $\nabla T_{appr}(\mathbf{x}) \approx \nabla T(\mathbf{x})$.

We obtain from (2.1)-(2.4)

$$\Delta q - 2\nabla q \int_s^{\bar{s}} \nabla q d\tau + 2\nabla q \nabla T = 0, \quad (2.5)$$

$$q(\mathbf{x}, s) = \psi(\mathbf{x}, s), \forall (\mathbf{x}, s) \in \Gamma \times (A, \bar{s}), \quad (2.6)$$

where

$$\psi(\mathbf{x}, s) = \partial_s \ln \varphi(\mathbf{x}, s).$$

The problem (2.5), (2.6) is nonlinear. In addition both functions q and T are unknown here. Now the main question is *How to approximate well both functions q and T using (2.5), (2.6)?* Indeed, if we approximate them well (in a certain sense, specified below), then the target coefficient $a(\mathbf{x})$ would be reconstructed easily via backwards calculations, see section 3. An equation similar with (2.5) was derived in the convexification method [6],[8]. However the major difference between our method and the convexification is in the numerical solution of the problem (2.5), (2.6). Indeed, it is solution of this problem which represents the major difficulty here.

3 Layer Stripping With Respect to the Source Position

An analogue of the nonlinear equation of this section for a different CIP, in which the original PDE was either hyperbolic or parabolic was previously derived in [3].

3.1 Nonlinear equation

We approximate the function $q(x, s)$ as a piecewise constant function with respect to the pseudo frequency s . That is, we assume that there exists a partition

$$\underline{s} = s_N < s_{N-1} < \dots < s_1 < s_0 = \bar{s}, s_{i-1} - s_i = h$$

of the interval $[\underline{s}, \bar{s}]$ with sufficiently small grid step size h such that

$$q(\mathbf{x}, s) = q_n(\mathbf{x}) \text{ for } s \in [s_n, s_{n-1}).$$

Hence

$$\int_s^{\bar{s}} \nabla q(\mathbf{x}, \tau) d\tau = (s_{n-1} - s) \nabla q_n(\mathbf{x}) + h \sum_{j=1}^{n-1} \nabla q_j(\mathbf{x}), s \in (s_n, s_{n-1}]. \quad (3.1)$$

We approximate the boundary condition (2.6) as a piecewise constant function,

$$q_n(\mathbf{x}) = \psi_n(\mathbf{x}), \mathbf{x} \in \partial\Omega, \quad (3.2)$$

where

$$\psi_n(\mathbf{x}) = \frac{1}{h} \int_{s_n}^{s_{n-1}} \psi(\mathbf{x}, s) ds. \quad (3.3)$$

Hence, for $s \in [s_n, s_{n-1})$ equation (2.5) can be rewritten as

$$\tilde{L}_n(q_n) := \Delta q_n - 2\nabla q_n \cdot \left(h \sum_{j=1}^{n-1} \nabla q_j - \nabla T \right) - 2h(\nabla q_n)^2 = 0. \quad (3.4)$$

In sections 4 and 5 we address the question on how to solve equations (3.4) for functions q_n with the boundary conditions (3.2).

3.2 Reconstruction of the target coefficient

Suppose that functions $\{q_i\}_{i=1}^n$ are approximated via solving problems (3.2), (3.4) and that the tail function is also approximated. Then we reconstruct the target coefficient $a(\mathbf{x})$ by backwards calculations as follows. First, we reconstruct the function $v(\mathbf{x}, s_n)$ by (2.4) as

$$v(\mathbf{x}, s_n) = -h \sum_{j=1}^n q_j + T(\mathbf{x}). \quad (3.5)$$

In principle we can reconstruct the target coefficient a from (2.1). However, it is unstable to take second derivatives. Hence, we first reconstruct the function $u(\mathbf{x}, s_n)$ as

$$u(\mathbf{x}, s_n) = \exp[v(\mathbf{x}, s_n)]. \quad (3.6)$$

Next, we use equation (1.1) in the weak form as

$$- \int_{\Omega} \nabla u \nabla \eta_k d\mathbf{x} = \int_{\Omega} a u \eta_k d\mathbf{x}, \quad (3.7)$$

where the test function $\eta_k(\mathbf{x})$, $k = 1, \dots, K$ is a quadratic finite element of a computational mesh with $\eta_k(\mathbf{x})|_{\partial\Omega} = 0$. The number K is finite and depends on the mesh we choose. Equalities (3.7) lead to a linear algebraic system which we solve. Then we obtain the function $(au)(\mathbf{x})$,

$$(au)(\mathbf{x}) \approx \sum_{k=1}^K \alpha_k \eta_k(\mathbf{x}).$$

Hence,

$$a(\mathbf{x}) \approx \frac{1}{u(\mathbf{x}, s_n)} \sum_{k=1}^K \alpha_k \eta_k(\mathbf{x}). \quad (3.8)$$

4 The Tail Function

We consider in this section two procedures for obtaining sequential approximations for the tail function. First we find a first guess for the tail function using the asymptotic behavior of the solution of the problem (1.1), (1.2) as $|\mathbf{x}_0| \rightarrow \infty$, as well as boundary measurements. Second, we describe an iterative procedure with respect to tails. We call the combination of these two procedures “accelerators”, because they help us to accelerate convergence of our method. We stress that we cannot prove convergence of the second procedure. However,

we have observed it in our numerical experiments. In our numerical experiments we have worked only with a rectangular domain. Hence, we assume in this section that

$$(x, z) \in \Omega := \{(x, z) : x_1 < x < x_2, z_0 < z < B\}.$$

However, we do not yet know how to address the issue of tails in the case of an arbitrary convex domain Ω .

4.1 The first guess for tails

First, we construct an approximation called "asymptotic tail". This is our first accelerator. We consider the fundamental solution of the problem (1.1), (1.2) for the case $a(x, z) \equiv k^2$. This solution is

$$u_0 = \frac{1}{2\pi} K_0(k|(x - s, z - B)|),$$

where $K_0(z)$ a modified Bessel function. It is well known that the asymptotic behavior of this function is

$$K_0(z) = \sqrt{\frac{\pi}{2|z|}} e^{-k|z|} (1 + O(\frac{1}{|z|})), |z| \rightarrow \infty. \quad (4.1)$$

Represent now solution of the problem (1.1), (1.2) as the solution of the following integral equation

$$u(x, z, s) = \frac{1}{2\pi} K_0(k|(x - s, z - z_m)|) - \frac{1}{2\pi} \int_{\Omega} K_0 \left(k \sqrt{(x - \xi)^2 + (z - \eta)^2} \right) [a(\xi, \eta) - k^2] u(\xi, \eta, s) d\xi d\eta. \quad (4.2)$$

Let $S(x, z, s) = |(x, z) - (s, z_m)|$. The geometric meaning of S is illustrated in Figure 1. Introducing the function

$$U(x, z, s) = 2\sqrt{2\pi S} e^{kS} \cdot u(x, z, s)$$

and taking into account (4.1) and (4.2), we obtain that

$$u(x, z, s) = \sqrt{\frac{\pi}{2S}} e^{-kS} \left[1 + \tilde{g}(x, z) + O\left(\frac{1}{S}\right) \right], S \rightarrow \infty.$$

The function $\tilde{g}(x, z)$ is unknown and is independent of S as $S \rightarrow \infty$. Hence, we obtain for the function $v = \ln u$

$$v(x, z, s) = -kS + \frac{1}{2} \ln\left(\frac{\pi}{2S}\right) + g(x, z) + O\left(\frac{1}{S}\right), S \rightarrow \infty, \quad (4.3)$$

where the unknown function $g(x, z)$ is derived from $\tilde{g}(x, z)$.

We approximate the function $g(x, z)$ by two different methods and the final answer is the average of two. The number of light sources $N = 3$ is taken in all our numerical experiments

when we approximate this function. We start at $z = z_0$ where the boundary values are known. We decompose the boundary values of v into

$$v(x, z_0, s_j) = -kS_j + \frac{1}{2} \ln\left(\frac{\pi}{2S_j}\right) + g_j(x, z_0) \quad (4.4)$$

for $j=1,2,3$. Then we average to obtain

$$g(x, z_0, s) = \frac{1}{3} \sum_{m=0}^3 g_j(x, z_0), \quad (4.5)$$

Note that in (4.5) one should actually put " \approx " sign instead of " $=$ ".

However, the above procedure (4.4)-(4.5) gives us the value of the tail functions $v(x, z, \bar{s})$ only at $z := z_0$, i.e., $v(x, z_0, \bar{s})$. Equation (4.3) provides an approximation for all $(x, z) \in \Omega$ if we simply set $g(x, z, s) = g(x, z_0, s)$. In our numerical experiments we found that this is insufficient. Hence, we use the measurement data from a different angle, which enhances our numerical results. We obtain a similar tail function using the measurement data at the lower edge of Ω , i.e., at $x = x_1$ and got a second tail function using the idea similar with the above. Thus, we have approximated $v(x_1, z, \bar{s})$. Finally we set for the first guess for producing a tail function

$$T_{1,0}(x, z, \bar{s}) := \frac{1}{2} [v(x, z_0, \bar{s}) + v(x_1, z, \bar{s})]. \quad (4.6)$$

4.2 The second accelerator: iterations with respect to tails

The second accelerator involves another iterative process that enhances the reconstructed inclusion. Recall that $k^2 := a_0$ is the constant background outside of our domain Ω' . We now show how to find an approximation $T_1(x, z, \bar{s})$ for the tail function. Let $u_{1,0} = e^{v_0}$ where $v_0 = T_{1,0}(x, z, \bar{s})$ is the function introduced above. We reconstruct the approximation $a_{1,1}(x, z)$ for the unknown coefficient $a(x, z)$ using the tail function (4.6) through the inversion formula in equation (3.7) for all quadratic finite element η_k :

$$-\int_{\Omega} \nabla u_{1,0} \nabla \eta_k d\mathbf{x} = \int_{\Omega} a_{1,1} u_{1,0} \eta_k d\mathbf{x}.$$

Next, we apply (3.8). Then on the second step we solve the following boundary value problem

$$\begin{aligned} \Delta u_{1,1} - a_{1,1}(x, z) u_{1,1} &= 0, (x, z) \in \Omega, \\ u_{1,1} |_{\partial\Omega} &= \varphi(\mathbf{x}, \bar{s}). \end{aligned}$$

The reason for doing so is that we need to satisfy the boundary condition obtained from measurements.

We now describe a heuristic idea which motivates our iterative scheme. Let the function u be the solution of the following boundary value problem

$$\Delta u - a(x, z) u = -\delta(x, z), (x, z) \in \Omega,$$

$$u|_{\partial\Omega} = \varphi(\mathbf{x}, \bar{s})$$

with the unknown coefficient $a(x, z)$ and the function u_0 satisfies

$$\Delta u_0 - a_0 u_0 = -\delta(x, z), (x, z) \in \Omega,$$

$$u_0|_{\partial\Omega} = \varphi(\mathbf{x}, \bar{s})$$

with the background function $a_0 = k^2$. Denote $p = u - u_0$. Then

$$\Delta p - a(x, z)p = (a(x, z) - a_0)u_0,$$

$$p|_{\partial\Omega} = 0.$$

Motivated by this idea, we introduce an iterative scheme and repeat the procedure until it converges. Suppose that after $m - 1$ iterations we have constructed the function $u_{1,m-1}$ and have found the approximation $a_{1,m}(x, z) > 0, m \geq 1$ for the unknown coefficient $a(x, z)$ using equation (3.7)-(3.8). Then on the iteration number m , we solve the following boundary value problem:

$$\Delta p_{1,m} - a_{1,m}(x, z)p_{1,m} = (a_{1,m}(x, z) - a_{1,m-1}(x, z))u_{1,m-1},$$

$$p_{1,m}|_{\partial\Omega} = 0.$$

Next, we set

$$u_{1,m} = u_{1,m-1} + p_{1,m}.$$

To accelerate convergence, we modify the iterative scheme slightly to solve the following boundary value problems:

$$\Delta p_{1,m} - a_{1,m}(x, z)p_{1,m} = \lambda_m (a_{1,m}(x, z) - a_{1,m-1}(x, z))u_{1,m-1}$$

where

$$\lambda_m = \frac{\exp\{\pi^2 e^{-(m-1)} (a_{1,m}(x, z) - a_{1,m-1}(x, z))^2\}}{\gamma^m}$$

and $\gamma = 1.05$. This choice of λ_m is made in numerical experiments. The choice of λ_m makes the sequence converge after about 50 iterations, instead of more than 300 in cases where $\lambda_m \equiv 1$.

Once we have $u_{1,m} = u_{1,m-1} + p_{1,m}$, we construct $a_{1,m+1}$ by equation (3.7) in the form of

$$-\int_{\Omega} \nabla u_{1,m} \nabla \eta_l d\mathbf{x} = \int_{\Omega} a_{1,m+1} u_{1,m} \eta_l d\mathbf{x},$$

for all quadratic finite elements $\eta_l, l = 1, \dots, K$ and use (3.8) then. We iterate until the process converges, i.e.,

$$\frac{\|a_{1,m_1} - a_{1,m_1-1}\|_{L_2(\Omega)}}{\|a_{1,m_1-1}\|_{C(\bar{\Omega})}} \leq \varepsilon$$

for a small $\varepsilon > 0$ of our choice, see (7.1) for a detail. We set for the first approximation for the unknown coefficient

$$a_1(x, z) := a_{1,m_1}(x, z).$$

Then we set for the tail

$$T_1(x, z, \bar{s}) = \ln u_{1,m_1}(x, z), \quad (4.7)$$

assuming that $u_{1,m_1} > 0$. Then we proceed with calculating the functions q_n as in section 5.

Remarks 4.1. 1. Unfortunately we cannot yet prove that functions $a_{1,m} > 0$. Therefore, we cannot prove analytically neither the existence of solutions of the above Dirichlet boundary value problems for functions $p_{1,m}$ nor the positivity of functions $u_{1,m}$. Neither we cannot analytically prove that functions $u_{1,m}$ converge, nor that our tail T_1 is close to the correct tail T . Nevertheless, we observe all these "nice" properties in our computations. Figure 2 displays the comparison of graphs of tails side by side, they have little visible difference. 2. Unlike [3], we do not change tails in all subsequent steps when calculating functions q_n . In other words, the tail function is kept the same $T := T_1(x, z, \bar{s})$ in all follow up steps of our algorithm.

5 The Algorithm for Approximating Functions q_n

Step 1. We need to find an approximation for the function q_1 . To do this, we solve equation (3.4) with the boundary condition (3.2) at $n = 1$ iteratively for q_1 . That is, we should solve

$$\Delta q_1 + 2\nabla q_1 \nabla T_1 = 2h(\nabla q_1)^2 \quad (5.1)$$

$$q_1(\mathbf{x}) = \bar{\psi}_1(\mathbf{x}), \mathbf{x} \in \partial\Omega, \quad (5.2)$$

We solve the problem (5.1), (5.2) iteratively as

$$\Delta q_{1,k} + 2\nabla q_{1,k} \nabla T_1 - 2h\nabla q_{1,k} \nabla q_{1,k-1} = 0, q_{1,k}(\mathbf{x}) = \bar{\psi}_1(\mathbf{x}), \mathbf{x} \in \partial\Omega \quad (5.3)$$

where $q_{1,0} = 0$.

We proceed with calculating the function $q_{1,m+1}$ as in (5.3). We iterate in (5.3) until the process converges, i.e.,

$$\|q_{1,k_1} - q_{1,k_1-1}\|_{L_2(\Omega)} \leq \varepsilon$$

for a small $\varepsilon > 0$ of our choice, and ε is the same as in (4.13). We set $q_1 := q_{1,k_1}$. The next reconstruction $a_2(x, z)$ is obtained using equations (3.5)-(3.8), where $T := T_1$.

Step n. We now find an approximation for the function q_n assuming that functions q_1, \dots, q_{n-1} are found. We solve iteratively equation (3.4) with the boundary condition (3.2) as follows

$$\Delta q_{n,k} - 2h \sum_{j=1}^{n-1} \nabla q_j \cdot \nabla q_{n,k} + 2\nabla q_{n,k} \nabla T_1 - 2h\nabla q_{n,k} \nabla q_{n,k-1} = 0, k = 1, \dots, m_n, \quad (5.4)$$

$$q_{n,k}(\mathbf{x}) = \psi_n(\mathbf{x}), \mathbf{x} \in \partial\Omega, \quad (5.5)$$

where $q_{n,0} := q_{n-1}$. We iterate until the process converges, i.e., until

$$\|q_{n,k_n} - q_{n,k_n-1}\|_{L_2(\Omega)} \leq \varepsilon$$

for the above small $\varepsilon > 0$. We set $q_n := q_{n,k_n}$. Then $a_{n+1}(x, z)$ is reconstructed using equations (3.5)-(3.8), $T := T_1$.

We find functions a_1, \dots, a_N for $n = 1, \dots, N$, where N is the number of subintervals of the interval $[s_0, \bar{s}]$. Finally, the resulting function $a(x, z)$ is

$$a(x, z) = \frac{1}{N} \sum_{i=1}^N a_i(x, z). \quad (5.6)$$

We stress that we did not prove convergence of tails T_n nor q_n rigorously. Neither we cannot prove that functions $p_{n,m}$ in section 4 are positive, because we cannot prove that $a_{n,m} - a_{n,m-1} < 0$ (in order to apply the maximum principle). However, we have observed both the positivity of functions $p_{n,m}$ and convergence of tails T_n and q_n in our computations.

6 Convergence

Below we follow the concept of Tikhonov for ill-posed problems [10], which is one of backbones of this theory. By this concept one should assume first that there exists an “ideal” exact solution of the problem with the exact data. Next, one should assume the presence of an error in the data of the level ζ , where $\zeta > 0$ is a small parameter. Suppose that an approximate solution is constructed for each sufficiently small ζ . This solution is called a “regularized solution”, if the ζ -dependent family of these solutions tends to that exact solution as ζ tends to zero. Hence, one should prove this convergence (Theorem 6.1).

In this section we use the Schauder’s theorem to estimate functions $q_{n,k}$, see §1 of Chapter 3 of [7] for this theorem. Since the Schauder’s theorem requires $C^{2+\alpha}$ smoothness of the boundary $\partial\Omega$, we assume in this section that $\Omega \subset \mathbb{R}^2$ is a convex bounded domain with $\partial\Omega \in C^{2+\alpha}$. This is, of course in a disagreement with the above case of Ω being a rectangle. However, we use the rectangle only because of the problem with tails, in which we cannot rigorously prove that they are small and do not yet know how to approximate them well heruistically for the case of a more general domain, so that they would be close to correct tails. However, an analogue of our convergence result (Theorem 6.1) can be proven for the case when Ω is rectangle and an FEM (i.e., discrete) version of equation (3.4) is considered with a fixed number R of finite elements. To do this, one needs to consider the weak formulation of (3.4) and to use the Lax-Milgram theorem instead of the Schauder’s theorem. Although the Lax-Milgram theorem would provide only estimates of H^1 norms of functions q_n rather than more desirable C^2 norms, but using the equivalency of norms in finite dimensional spaces, we can still get estimates of C^2 norms and these estimates would naturally depend on R .

6.1 Exact solution

Following the Tikhonov concept, we need to introduce the definitions of the exact solution first. We assume that there exists an exact coefficient function $a^*(x) \in C^\alpha(\overline{\Omega})$, $\alpha = \text{const.} \in (0, 1)$, which is a solution of our Inverse Problem. Let the function

$$u^*(\mathbf{x}, s) \in C^{2+\alpha}(|\mathbf{x} - \mathbf{x}_0| \geq \varepsilon), \forall \varepsilon > 0, \forall \mathbf{x}_0 = (s, B) > 0, \forall s \in [\underline{s}, \overline{s}]$$

be the solution of the problem (1.1), (1.2) with $a(\mathbf{x}) := a^*(\mathbf{x})$. Let

$$v^*(\mathbf{x}, s) = \ln u^*(\mathbf{x}, s), q^*(\mathbf{x}, s) = \frac{\partial v^*(\mathbf{x}, s)}{\partial s}, T^*(\mathbf{x}, \overline{s}) = v^*(\mathbf{x}, \overline{s}).$$

By (2.1)

$$a^*(\mathbf{x}) = \Delta v^* + (\nabla v^*)^2. \quad (6.1)$$

Also, the function q^* satisfies the following analogue of equation (2.5)

$$\Delta q^* - 2\nabla q^* \cdot \int_s^{\overline{s}} \nabla q^*(x, \tau) d\tau + 2\nabla q^* \nabla T^* = 0 \quad (6.2)$$

with the boundary condition (see (2.6))

$$q^*(\mathbf{x}, s) = \psi^*(\mathbf{x}, s), (\mathbf{x}, s) \in \partial\Omega \times [\underline{s}, \overline{s}], \quad (6.3)$$

where $\psi^*(\mathbf{x}, s) = \partial_s \ln \varphi^*(\mathbf{x}, s)$, where $\varphi^*(\mathbf{x}, s) = u^*(\mathbf{x}, s)$ for $(\mathbf{x}, s) \in \partial\Omega \times [\underline{s}, \overline{s}]$.

Definition. We call the function $q^*(\mathbf{x}, s)$ the *exact solution* of the problem (2.5), (2.6) with the *exact boundary* condition $\psi^*(x, s)$. Naturally, the function $a^*(\mathbf{x})$ from (6.1) is called the *exact solution* of our Inverse Problem.

Therefore,

$$q^*(\mathbf{x}, s) \in C^{2+\alpha}(\overline{\Omega}) \times C^1[\underline{s}, \overline{s}]. \quad (6.4)$$

We now approximate the function $q^*(x, s)$ via a piecewise constant function with respect to $s \in [\underline{s}, \overline{s}]$. Let

$$q_n^*(\mathbf{x}) = \frac{1}{h} \int_{s_n}^{s_{n-1}} q^*(\mathbf{x}, s) ds, \quad \psi_n^*(\mathbf{x}) = \frac{1}{h} \int_{s_n}^{s_{n-1}} \psi^*(x, s) ds$$

Then by (6.4)

$$q^*(x, s) = q_n^*(x) + Q_n(x, s), \quad \psi^*(x, s) = \psi_n^*(x) + \Psi_n(x, s), \quad (6.5)$$

$s \in [s_n, s_{n-1}]$, where functions Q_n, Ψ_n are such that for $s \in [s_n, s_{n-1}]$

$$\|Q_n(\mathbf{x}, s)\|_{C^{2+\alpha}(\overline{\Omega})} \leq C^* h, \quad \|\Psi_n(\mathbf{x}, s)\|_{C^{2+\alpha}(\overline{\Omega})} \leq C^* h, \quad \forall s \in [s_n, s_{n-1}], \quad n = 1, \dots, N, \quad (6.6)$$

where the constant $C^* > 0$ depends only on $C^{2+\alpha}(\overline{\Omega}) \times C^1[\underline{s}, \overline{s}]$ and $C^{2+\alpha}(\partial\Omega) \times C^1[\underline{s}, \overline{s}]$ norms of functions q^* and ψ^* respectively. Hence

$$q_n^*(\mathbf{x}) = \psi_n^*(\mathbf{x}), \mathbf{x} \in \partial\Omega \quad (6.7)$$

and the following analogue of equation (3.4) holds

$$\tilde{L}_n(q_n) := \Delta q_n^* - 2\nabla q_n^* \cdot \left(h \sum_{j=1}^{n-1} \nabla q_j^* - \nabla T^* \right) - 2h(\nabla q_n^*)^2 = F_n^*(\mathbf{x}, h). \quad (6.8)$$

where the function $F_n(\mathbf{x}, h) \in C^\alpha(\overline{\Omega})$ and

$$\|F_n^*(\mathbf{x}, h)\|_{C^\alpha(\overline{\Omega})} \leq C^*h. \quad (6.9)$$

We also assume that the data $\varphi(\mathbf{x}, s)$ in (1.3) are given with an error. This naturally produces an error in the function $\psi(\mathbf{x}, s)$ in (2.6). An additional error is introduced due to taking the average value of $\psi(\mathbf{x}, s)$ over the interval (s_n, s_{n-1}) . Hence, it is reasonable to assume that

$$\left\| \overline{\psi}_n^*(\mathbf{x}) - \psi_n(\mathbf{x}) \right\|_{C^{2+\alpha}(\partial\Omega)} \leq C_1(\sigma + h), \quad (6.10)$$

where $\sigma > 0$ is a small parameter characterizing the level of the error in the data $\psi(\mathbf{x}, s)$ and the constant $C_1 > 0$ is independent on numbers σ , h and n .

Remark 6.1. It should be noted that usually the data $\varphi(\mathbf{x}, s)$ in (1.3) are given with a random noise. Although the differentiation of the noisy data is an ill-posed problem, but there exist effective numerical regularization methods of its solution. We are not addressing the corresponding theory here referring the reader to e.g., [4], and also see section 7 for our way of handling it.

6.2 Convergence theorem

First, we reformulate the Schauder's theorem in a way, which is convenient for our case. Introduce the positive constant M^* as

$$M^* = \left\{ \left[\max_{1 \leq n \leq N} \left(\|q_n^*\|_{C^{1+\alpha}(\overline{\Omega})} \right) + 2 \|T^*\|_{C^{1+\alpha}(\overline{\Omega})} + \|\nabla q_1^*\|_{C^\alpha(\overline{\Omega})}^2 + 1 \right], C^*, C_1 \right\},$$

where C^* and C_1 are constants from (6.9) and (6.10) respectively. Consider the Dirichlet boundary value problem

$$\begin{aligned} \Delta u + \sum_{j=1}^3 b_j(x)u_{x_j} - d(x)u &= f(x), \quad x \in \Omega, \\ u|_{\partial\Omega} &= g(x), \quad g \in C^{2+\alpha}(\partial\Omega), \end{aligned}$$

where functions

$$b_j, d, f \in C^\alpha(\bar{\Omega}), d(x) \geq 0; \max\left(\|b_j\|_{C^\alpha(\bar{\Omega})}, \|d\|_{C^\alpha(\bar{\Omega})}\right) \leq 4M^*.$$

By the Schauder theorem there exists unique solution $u \in C^{2+\alpha}(\bar{\Omega})$ of this problem and with a constant $K = K(M^*, \Omega) > 0$ the following estimate holds

$$\|u\|_{C^{2+\alpha}(\bar{\Omega})} \leq K \left[\|g\|_{C^{2+\alpha}(\partial\Omega)} + \|f\|_{C^\alpha(\bar{\Omega})} \right].$$

In Theorem 6.1 we use a function $T_{appr}(x, z, \bar{s})$ instead of the above constructed function $T_1(x, z, \bar{s})$ only because the latter was constructed for a rectangle, while Theorem 6.1 works with a convex bounded domain, also see the beginning of this section.

Theorem 6.1. *Let $\Omega \subset \mathbb{R}^2$ be a convex bounded domain with the boundary $\partial\Omega \in C^3$. Suppose that an approximation $T_{appr}(x, z, \bar{s})$ for the tail is constructed in such a way that*

$$\|T_{appr} - T^*\|_{C^{2+\alpha}(\bar{\Omega})} \leq \xi, \quad (6.11)$$

where $\xi \in (0, 1)$ is a sufficiently small number and that this function $T_{appr}(x, z, \bar{s})$ is used in (5.3), (5.4) instead of the function $T_1(x, z, \bar{s})$. Denote $\eta = h + \sigma + \xi + \varepsilon$. Suppose that the number $\beta := \bar{s} - s_0 = Nh$ is such that

$$\beta \leq \frac{1}{48KM^*}. \quad (6.12)$$

Then there exists a sufficiently small number $\eta_0 = \eta_0(K(M^*, \Omega), M^*, c, \underline{s}, \bar{s}) \in (0, 1)$ and a sufficiently large small number $h_0 = h_0(K(M^*, \Omega), M^*, c, \underline{s}, \bar{s}) \in (0, 1)$ such that for all $\eta \in (0, \eta_0)$ and for every integer $n \in [1, N]$ the following estimates hold

$$\|q_n - q_n^*\|_{C^{2+\alpha}(\bar{\Omega})} \leq 2KM^*(h + 3\eta), \quad (6.13)$$

$$\|q_n\|_{C^{2+\alpha}(\bar{\Omega})} \leq 2M^*. \quad (6.14)$$

Remark 6.2. As it was stated above, unlike the time dependent case of [3], we cannot prove the estimate (6.11) for tails. However, we observe convergence of tails in computations if taking $T := T_1$ as in (4.7).

6.3 Proof of Theorem 6.1

In the course of this proof we assume that $\eta \in (0, \eta_0)$, $h \in (0, \eta_0)$. Denote

$$\tilde{q}_{n,k}(\mathbf{x}) = q_{n,k}(\mathbf{x}) - q^*(\mathbf{x}), \tilde{T}(\mathbf{x}) = T_{appr}(\mathbf{x}) - T^*(\mathbf{x}), \tilde{\psi}_n = \psi_n - \psi_n^*, \quad (6.16)$$

$$v_{n,k}(\mathbf{x}, s_n) = -hq_{n,k} - h \sum_{j=1}^{n-1} q_j + T_{appr}(\mathbf{x}), u_{n,k}(\mathbf{x}, s_n) = \exp[v_{n,k}(\mathbf{x}, s_n)], \quad (6.17)$$

$$\tilde{v}_{n,k}(\mathbf{x}, s_n) = v_{n,k}(\mathbf{x}, s_n) - v_n^*(\mathbf{x}, s_n), \tilde{a}_{n,k}(\mathbf{x}) = a_{nk}(\mathbf{x}) - a^*(\mathbf{x}). \quad (6.18)$$

The proof basically consists in estimating these differences.

First, we estimate $\tilde{q}_{1,1}$. Set in (6.8) $n = 1$ and subtract it from (5.3) at $k = 1$, recalling that $q_{1,0} = 0$. We obtain

$$\begin{aligned} \Delta \tilde{q}_{1,1} - 2\nabla \tilde{q}_{1,1} \nabla T_{appr} &= 2\nabla q_1^* \nabla \tilde{T} - 2h(\nabla q_1^*)^2 - F_1^*, \\ \tilde{q}_{1,1} |_{\partial\Omega} &= \tilde{\psi}_1. \end{aligned}$$

By Schauder theorem, and (6.9)-(6.11) we obtain

$$\|\tilde{q}_{1,1}\|_{C^{2+\alpha}(\bar{\Omega})} \leq KM^*(h + \eta). \quad (6.19)$$

Hence,

$$\|\tilde{q}_{1,1} + q_1^*\|_{C^{2+\alpha}(\bar{\Omega})} = \|q_{1,1}\|_{C^{2+\alpha}(\bar{\Omega})} \leq M^* + KM^*(h + \eta) \leq 2M^*. \quad (6.20)$$

Now we estimate $\tilde{q}_{1,k}$. Set in (6.8) $n = 1$ and subtract it from (5.3). Then

$$\begin{aligned} \Delta \tilde{q}_{1,k} + 2(\nabla T_{appr} - h\nabla q_{1,k-1}) \nabla \tilde{q}_{1,k} &= \\ -2\nabla q_1^* \left(\nabla \tilde{T} - 2h\nabla \tilde{q}_{1,k-1} \right) - F_1^*, \end{aligned} \quad (6.21)$$

and also

$$\tilde{q}_{1,k} |_{\partial\Omega} = \tilde{\psi}_1. \quad (6.22)$$

Set in (6.21) $k = 2$. Then (6.19) and (6.20) imply that

$$\|2(\nabla T_{appr} - h\nabla q_{1,1})\|_{C^\alpha(\bar{\Omega})} \leq 2(M^* + 2hM^*) \leq 3M^*, \quad (6.23)$$

$$\left\| 2\nabla q_1^* \left(\nabla \tilde{T} - 2h\nabla \tilde{q}_{1,1} \right) + F_1^* \right\|_{C^\alpha(\bar{\Omega})} \leq 2M^* [\xi + 2KM^*h(h + \eta) + \eta/2].$$

By (6.12) $2KM^*h < 1/2$. Hence,

$$\left\| 2\nabla q_1^* \left(\nabla \tilde{T} - 2h\nabla \tilde{q}_{1,1} \right) + F_1^* \right\|_{C^\alpha(\bar{\Omega})} \leq 2M^*(h + 2\eta).$$

Hence, by (6.21)-(6.23) and Schauder's theorem

$$\|\tilde{q}_{1,2}\|_{C^{2+\alpha}(\bar{\Omega})} \leq 2KM^*(h + 3\eta).$$

and similarly with (6.19)

$$\|q_{1,2}\|_{C^{2+\alpha}(\bar{\Omega})} \leq 2M^*.$$

Assume that

$$\|\tilde{q}_{1,k-1}\|_{C^{2+\alpha}(\bar{\Omega})} \leq 2KM^*(h + 3\eta), \|q_{1,k-1}\|_{C^{2+\alpha}(\bar{\Omega})} \leq 2M^*. \quad (6.24)$$

We now estimate the function $\tilde{q}_{1,k-1}$. Similarly with the above

$$\|2(\nabla T_{appr} - h\nabla q_{1,k-1})\|_{C^\alpha(\bar{\Omega})} \leq 2(M^* + 2hM^*) \leq 6M^*. \quad (6.25)$$

Next, using (6.24), we obtain

$$\left\| 2\nabla q_1^* \left(\nabla \tilde{T} - 2h\nabla \tilde{q}_{1,k-1} \right) + F_1^* \right\|_{C^\alpha(\bar{\Omega})} \leq 2M^* [\xi + 2KM^*h(h + \eta) + \eta/2].$$

By (6.12) $2KM^*h(h + \eta) < 1/2(h + \eta)$. Hence,

$$\xi + 2KM^*h(h + \eta) + \eta/2 \leq h + 2\eta.$$

Hence,

$$\left\| 2\nabla q_1^* \left(\nabla \tilde{T} - 2h\nabla \tilde{q}_{1,k-1} \right) + F_1^* \right\|_{C^\alpha(\bar{\Omega})} \leq 2M^*(h + 2\eta). \quad (6.26)$$

Hence, Schauder's theorem, (6.21), (6.25) and (6.26) lead to

$$\|\tilde{q}_{1,k}\|_{C^{2+\alpha}(\bar{\Omega})} \leq 2KM^*(h + 3\eta), \|q_{1,k-1}\|_{C^{2+\alpha}(\bar{\Omega})} \leq 2M^*, k = 1, 2, \dots \quad (6.27)$$

We now estimate the function $\tilde{q}_{n,k}$, assuming that (6.27) holds for functions \tilde{q}_i, q_i with $j < n$, as well as for functions $\tilde{q}_{n,m}, q_{n,m}$ with $m \leq k - 1$. In other words, we assume that

$$\|\tilde{q}_j\|_{C^{2+\alpha}(\bar{\Omega})} \leq 2KM^*(h + 3\eta), \|q_j\|_{C^{2+\alpha}(\bar{\Omega})} \leq 2M^*. \quad (6.28)$$

and

$$\|\tilde{q}_{n,m}\|_{C^{2+\alpha}(\bar{\Omega})} \leq 2KM^*(h + 3\eta), \|q_{n,m}\|_{C^{2+\alpha}(\bar{\Omega})} \leq 2M^*, m \leq k - 1. \quad (6.29)$$

Subtracting (6.8) from (5.4) and using (5.5), (6.3) and (6.16), we obtain

$$\Delta \tilde{q}_{n,k} - 2 \left(h \sum_{j=1}^{n-1} \nabla q_j - (\nabla T_{appr} - 2h\nabla q_{n,k-1}) \right) \nabla \tilde{q}_{n,k} = \quad (6.30)$$

$$2 \left(h \sum_{j=1}^{n-1} \nabla \tilde{q}_j \right) \nabla q_n^* + 2\nabla q_n^* \nabla \tilde{T} + 2h\nabla q_n^* \nabla \tilde{q}_{n,k-1},$$

$$\tilde{q}_{n,k} |_{\partial\Omega} = \tilde{\psi}_n. \quad (6.31)$$

Estimate first the coefficient at $\nabla \tilde{q}_{n,k}$ in (6.30). Using (6.28) and (6.29), we obtain

$$2 \left\| h \sum_{j=1}^{n-1} \nabla q_j \right\|_{C^\alpha(\bar{\Omega})} \leq 4M^*Nh,$$

$$2 \|\nabla T_{appr} - 2h\nabla q_{n,k-1}\|_{C^\alpha(\bar{\Omega})} \leq 2(M^* + 2hM^*) \leq 3M^*.$$

Since by (6.12) $4M^*\bar{N}h \leq M^*$, then the estimate for that coefficient is

$$2 \left\| h \sum_{j=1}^{n-1} \nabla q_j \right\|_{C^\alpha(\bar{\Omega})} + 2 \|\nabla T_{appr} - 2h\nabla q_{n,k-1}\|_{C^\alpha(\bar{\Omega})} \leq 4M^*. \quad (6.32)$$

Hence, we can apply Schauder's theorem with the constant K . Now we estimate the right hand side of equation (6.30). Using (6.28) and (6.29), we obtain

$$\begin{aligned} \left\| 2 \left(h \sum_{j=1}^{n-1} \nabla \tilde{q}_j \right) \nabla q_n^* \right\|_{C^\alpha(\bar{\Omega})} &\leq 4K (M^*)^2 N h (h + 3\eta), \\ \|2h\nabla q_n^* \nabla \tilde{q}_{n,k-1}\|_{C^\alpha(\bar{\Omega})} &\leq 4K (M^*)^2 h (h + 3\eta), \\ \left\| 2\nabla q_n^* \nabla \tilde{T} \right\|_{C^\alpha(\bar{\Omega})} &\leq 2M^*\eta. \end{aligned}$$

Estimate the right hand sides of the last three inequalities. By (6.12) we have

$$\begin{aligned} 4K (M^*)^2 \bar{N} h (h + 3\eta) &\leq \frac{M^*}{12} (h + 3\eta), \\ 4K (M^*)^2 h (h + 3\eta) &\leq \frac{M^*}{12} (h + 3\eta). \end{aligned}$$

Hence,

$$\begin{aligned} \left\| 2 \left(h \sum_{j=1}^{n-1} \nabla \tilde{q}_j \right) \nabla q_n^* \right\|_{C^\alpha(\bar{\Omega})} + \|2h\nabla q_n^* \nabla \tilde{q}_{n,k-1}\|_{C^\alpha(\bar{\Omega})} + \|2h\nabla q_n^* \nabla \tilde{q}_{n,k-1}\|_{C^\alpha(\bar{\Omega})} &\quad (6.33) \\ &\leq \frac{M^*}{6} (h + 3\eta) + 2M^*\eta = M^* \left(\frac{h}{6} + \frac{3}{2}\eta \right). \end{aligned}$$

By (6.30)-(6.33) and Schauder theorem we obtain

$$\|\tilde{q}_{n,k}\|_{C^{2+\alpha}(\bar{\Omega})} \leq KM^* \left(\frac{h}{6} + \frac{3}{2}\eta \right) + K\eta \leq KM^* \left(\frac{h}{6} + \frac{5}{2}\eta \right) \leq KM^* (h + 3\eta). \quad (6.34)$$

Hence,

$$\|q_{n,k}\|_{C^{2+\alpha}(\bar{\Omega})} = \|\tilde{q}_{n,k} + q_n^*\|_{C^{2+\alpha}(\bar{\Omega})} \leq KM^* (h + 3\eta) + M^* \leq 2M^*. \quad (6.35)$$

Estimates (6.34) and (6.35) complete the proof of this theorem. \square

7 Numerical Studies

We have performed numerical experiments on several cases of reconstructions using the method discussed above. We have chosen the range of geometrical parameters of the rectangle Ω , which is typical for optical imaging of small animals and have chosen the range of optical parameters typical for biological tissues [1],[11],[13].

7.1 Some Details of Numerical Studies

For the forward problem, we calculate the solution of the diffusion equation

$$D\Delta u - \mu_a(x, z)u = -\delta(x - s, z - z_m) \quad (7.1)$$

with the conventional condition at the infinity

$$\lim_{|(x,z)| \rightarrow \infty} u(x, z, s) = 0, \quad (7.2)$$

where $D = 1/(3\mu'_s) \equiv \text{const.} > 0$ is the diffusion coefficient, where optical coefficients μ'_s and $\mu_a(x, z)$ were discussed in Introduction (Section 1). In our computations the function $\mu_a(x, z)$ is unknown and the constant μ'_s is given. Thus, in our case $a(x, z) = 3\mu'_s \cdot \mu_a(x, z)$ (compare with (1.4)). Consider the rectangle Ω ,

$$\Omega = \{(x, z) : 5\text{cm} < x < 15\text{cm}, 5\text{cm} < z < 10\text{cm}\}.$$

We assume that

$$a(x, z) = k^2 = \text{const.} > 0 \text{ in } \mathbb{R}^2 \setminus \Omega. \quad (7.3)$$

We assume that in (7.1) the source position (s, z_m) is running along the right side of Ω , i.e., $z_m = L = 10\text{cm}$. Also, consider a bigger rectangle

$$\Omega_0 = \{(x, z) : 0\text{cm} < x < 20\text{cm}, 0\text{cm} < z < 15\text{cm}\}.$$

The reason why we consider the rectangle Ω_0 along with the rectangle Ω is that it is natural to approximate the solution of the problem (7.1), (7.2) in the infinite domain by the solution of equation (7.1) in Ω_0 with Robin boundary conditions at $\partial\Omega_0$. We have established numerically that for the range of parameters we use the solution of the problem (7.1), (7.2) is close in Ω to the solution of equation (7.1) in the bigger rectangle Ω_0 with the Robin boundary conditions at its sides. Figure 3 illustrates rectangles Ω_0 and Ω .

The light sources are located in several positions $(x_i, z) = (s_i, 10)$ along the right-hand side of the smaller rectangle Ω , and receivers, which mimic the so-called CCD camera are located at the left-hand side of Ω . CCD stands for a “charge-coupled device”. A CCD camera is an image sensor, consisting of an integrated circuit containing an array of linked, or coupled, light-sensitive capacitors. A typical CCD camera can take up to 512×512 data points simultaneously, which will provide an adequate amount of data for our reconstruction. In all three examples, we have used an ideal light source modeled by the function $-\delta(x - s_i, z - 10)$ in the 2D case of (1.1). In numerical simulation $\delta(x - s_i, z - 10) = c\eta(s_i, 10)$, where η is the finite element at the location, and c is the scaling constant to ensure that the area equals one.

We use three (3) sources to construct an approximation of the tail functions which was described above. Next, we use all five (5) sources for the above layer stripping procedure both in the s -derivative and the s -integral.

We have generated the data for the forward problem for total of five (5) different locations of the light source, $s_i = 1, \dots, 5$, where $s_1 = 0, s_i = s_{i-1} + 0.625cm, i = 2, \dots, 5$. Hence, $N = 4$ and we have used four (4) functions q_n . An increase of the number N did not result in significant improvements of results. Note that a similar observation took place in numerical experiments of [3] for the case of an increase of the number of functions q_n after a certain “limit”. In our reconstruction method, we use the solution of the forward problem to generate the data for the inverse, add noise to the measurement data, and reconstruct the absorption coefficient $\mu_a(x, z)$ in Ω . The domain Ω will be our basic computational domain for our inverse calculations.

In our examples, the coefficients in equation (7.1) are $D = 0.02cm$ uniformly and $\mu_a = 0.1cm^{-1}$ at all grids except off the inclusions, and in inclusions μ_a ranges from 0.1 to $0.3 cm^{-1}$. The maximum inclusion/background contrast is 3:1 in our computations. Our algorithm calculates the forward problem with Robin boundary conditions at $\partial\Omega_0$, given the distribution of the absorption coefficient. A total of 130×93 rectangular finite elements is used for forward calculations for the domain Ω_0 .

For the simulated boundary measurements we take the solution of the forward problems along the left and lower boundaries of Ω to construct first guess for tails (section 4.1) and then we take all 4 sides for the rest of the problem. The number of measuring points is 65 along the left edge of Ω and 31 along the lower edge of Ω . The number of measuring points at the low left corner is shared by both sides and therefore the total number of independent measuring points is 95.

For each detector position, we introduce the random noise as the random process with respect to the detector locations, $\tilde{\varphi}(\mathbf{x}, s_k) = \varphi(\mathbf{x}, s_k) [1 + \chi(\mathbf{x})]$, where $\chi(\mathbf{x})$ is the random variable, which we introduce as $\chi = 0.02W$, where W is a white noise with equal distribution at $[-1,1]$. Hence, this is 2% of the multiplicative random noise. To obtain the realistic first s -derivatives, we started with simulated light distribution $u(x, z, s)$ added with similar noise to simulate the situation used in applications and let $v = \ln u$. Then we take first derivatives with respect to s as shown in the paragraph below.

A regularization method was introduced to pre-process the noise in the measurement data. We use a polynomial approximation with respect to the detector location \mathbf{x} . In our setting, the measurements are collected at 65 locations along the left boundary and 31 points along the lower boundary. We use an eight order polynomial to approximate functions $\tilde{\varphi}(\mathbf{x}, s_k)$ with respect to \mathbf{x} for each s_k . The polynomial is optimal in the least square sense [12],[14], and its sub-routine is commonly available, see for example

http://perso.orange.fr/jean-pierre.moreau/f_lstsq.html. We demonstrate the essence of the approximation in Figure 4. Thus, we have obtained approximate polynomial functions $\bar{\varphi}(x, s_k)$. We use functions $\bar{\varphi}(x, s_k)$ instead of $\varphi(x, s_k)$. The first s -derivatives are processed afterwards by the formula

$$f'(s_1) \approx \frac{f(s_2) - f(s_1)}{s_2 - s_1}.$$

and similar ones for other source locations.

7.2 Numerical Experiments

In the following numerical examples, we illustrate the results in a few different shapes and locations of the two inclusions. Our method has shown its success in dealing with those cases. In all cases, iterations with respect to tail (as described in section 4.2) were only done for the first light sources. Additional light sources did not bring any significant changes to reconstruction, therefore iterations with respect to tails are not shown in this paper. The total number of elements K in (3.8) is 450 in our calculation.

The Convergence Criterion for functions a_m in the procedure of finding the second accelerator T_1 for tails is

$$\|a_{1m_1}(x, z) - a_{1m_1-1}(x, z)\| \equiv \frac{\sqrt{\sum_{i=1, \dots, i_{max}, j=1, \dots, j_{max}} |(a_{1,m_1}(x_i, z_j) - a_{1,m_1-1}(x_i, z_j))|^2}}{\sqrt{N_1} \max |a_{1,m_1-1}(x_i, z_j)|} \leq \varepsilon, \quad (7.1)$$

where $N_1 = i_{max}j_{max}$ is the total number of finite elements. In all our examples, $\varepsilon = 10^{-5}$. The number of iterations required for convergence is listed below:

The number of iterations required for convergence

Example 1	Example 2	Example 3
52	50	48

Example 1. Inclusions are two circles with the radius 1 cm, and their centers are placed 2 cm off the left edge. The coefficient is $\mu_a(x, z) = 0.3$ inside inclusion and $\mu_a(x, z) = 0.1 = k^2$ outside of inclusions. We have also added 2% of random noise to the boundary measurements, see subsection 7.1.

Figure 5a displays the original distribution and its 1-d cross section. Figure 5b shows reconstruction from the noisy data and its 1-d cross section.

The relative errors of the reconstruction are as follows:

Table 1. The relative errors of reconstructions in Example 1

RMSE	AME	ME
0.312366805537619	0.115817263155519	-0.058254402556204

Note that for the data set $(x_1, x_2, \dots, x_{N_1})$ and its approximation $(\hat{x}_1, \hat{x}_2, \dots, \hat{x}_{N_1})$, the values of the function $\mu_a(x, z)$ taken at each of the grid points, the Relative Root Mean Square Error (RMSE), Relative Absolute Mean Error (MAE) and Relative Mean Error (ME) are calculated by

$$RMSE = \frac{\sqrt{\sum_{k=1}^{N_1} (x_k - \hat{x}_k)^2}}{\sqrt{N_1} \max |x_k|}, \quad MAE = \frac{\sum_{k=1}^{N_1} |x_k - \hat{x}_k|}{N_1 \max |x_k|}, \quad ME = \frac{\sum_{k=1}^{N_1} (x_k - \hat{x}_k)}{N_1 \max |x_k|}.$$

In our case x_k are correct values of the coefficient $\mu_a(x, z)$ at the grid points of the sub-rectangle

$$\Omega' = \{(x, z) : 5cm < x < 15cm, 5cm < z < 8cm\} \subset \Omega.$$

We illustrate in Figure 5c the difference of two consecutive reconstruction

$$\|a_m(x, z) - a_{m-1}(x, z)\| \equiv \frac{\sqrt{\sum_{i=1, \dots, i_{max}, j=1, \dots, j_{max}} |(a_m(x_i, z_j) - a_{m-1}(x_i, z_j))|^2}}{\sqrt{N_1} \max |a_{m-1}(x_i, z_j)|}$$

as a function of the number of iteration m . Figure 5d depicts the relative error in comparison with actual inclusion expressed by

$$RMSE \equiv \frac{\sqrt{\sum_{i=1, \dots, i_{max}, j=1, \dots, j_{max}} |(a_m(x_i, z_j) - a(x_i, z_j))|^2}}{\sqrt{N_1} \max |a(x_i, z_j)|}$$

as a function of the number of iterations m .

Example 2. Inclusions are two circles of the radius 1cm, and their centers are placed 2 cm off the left edge. The coefficient $\mu_a(x, z)$ is defined as

$$\mu_a(x, z) = \begin{cases} \max [0.3 \cos d(x, z), 0.1], & \text{inside of each circle} \\ 0.1 & \text{otherwise,} \end{cases} \quad (7.4)$$

where $d(x, z)$ is the minimum distance to center of each of these two circles.

Figure 6a displays the original function in two inclusions and its 1-d cross section. Figure 6b shows the reconstruction result with 2% noise and its 1-d cross section.

The relative errors of reconstruction are as follows:

Table 2. The relative errors of reconstruction in Example 2

$RMSE$	AME	ME
0.261946376827213	0.087514613280764	-0.024755081675791

We illustrate in Figure 6c the difference of two consecutive reconstruction $\|a_m(x, z) - a_{m-1}(x, z)\|$ as a function of the number of iteration m . Figure 6d depicts the relative error in comparison with actual inclusion expressed by $RMSE$ as a function of the number of iterations m .

Example 3. Inclusions are two circles of the radius 1 cm and 0.6 cm, whose centers are placed 2 cm off the left edge. The coefficient $\mu_a(x, z)$ is defined as

$$\mu_a(x, z) = \begin{cases} \max [0.3(\cos d(x, z)(1 + 0.1\eta(x, z))), 0.1], & \text{inside of each circle} \\ 0.1 & \text{otherwise.} \end{cases} \quad (7.5)$$

Similarly with (7.4) $d(x, z)$ is the distance to center of the circle. In (7.5) η is a realization of a white noise valued between $[-1, 1]$. The random pattern is introduced to test the ability of our method to handle complex shapes. See Figures 7a,b for results.

Table 3. The relative errors of reconstruction in Example 3

$RMSE$	AME	ME
0.336142461513025	0.084080392591033	-0.026699370402152

We illustrate in Figure 7c the difference of two consecutive reconstruction $\|a_m(x, z) - a_{m-1}(x, z)\|$ as a function of the number of iteration m . Figure 7d depicts the relative error in comparison with actual inclusion expressed by $RMSE$ as a function of the number of iterations m .

Acknowledgments

The work of all authors was supported by the National Institutes of Health grant #1R21Ns052850-01A1. The work of MK was also supported by the U.S. Army Research Laboratory and U.S. Army Research Office under contract/ grant number W911NF-05-1-0378.

References

1. S. Arridge, Optical tomography in medical imaging, *Inverse Problems*, 15, 841-893, 1999.
2. A.B. Bakushinsky, T. Khan and A. Smirnova, Inverse problem in optical tomography and its numerical investigation by iteratively regularized methods, *J. Inverse and Ill-Posed Problems*, 13, 537-551, 2005.
3. L. Beilina and M.V. Klibanov, A globally convergent numerical method for some coefficient inverse problems with resulting second order elliptic equations, submitted for publication, a preprint is available on line at http://www.ma.utexas.edu/mp_arc/index-07 (preprint number 07-311), at <http://www.math.ntnu.no/preprint/numerics/2007>, and at <http://www.math.uncc.edu/people/research/mklibanv.php>
4. Yu.A. Grazin, M.V. Klibanov and T.R. Lucas, Numerical solution of a subsurface imaging inverse problem, *SIAM J. Appl. Math.*, 62, 664-683, 2001.
5. E. Haber, U.M. Asher and D. Oldenburg, On optimization techniques for solving nonlinear inverse problems, *Inverse Problems*, 16, 1263-1280, 2000.
6. M.V. Klibanov and A. Timonov, *Carleman Estimates for Coefficient Inverse Problems and Numerical Applications*, VSP, Utrecht, 2004.
7. O.A. Ladyzhenskaya and N.N. Uralceva, *Linear and Quasilinear Elliptic Equations*, Academic Press, New York, 1969.
8. H. Shan, M.V. Klibanov, H. Liu, N. Pantong and J. Su, Numerical implementation of the convexification algorithm for an optical diffusion tomograph, *Inverse Problems*, 24, paper number 025026, 2008.
9. J. Su, H. Shan, H. Liu and M.V. Klibanov, Reconstruction method from a multiple-site continuous-wave source for three-dimensional optical tomography, *J. Optical Society of America A*, 23, 2388-2395, 2006.
10. A.N. Tikhonov and V.Ya. Arsenin, *Solutions of Ill-Posed Problems*, Winston& Sons, Washington, DC 1977.
11. R.R. Alfano, R.R. Pradhan and G.C. Tang, Optical spectroscopic diagnosis of cancer and normal breast tissues, *J. Opt. Soc. Am. B*, 6, 1015-1023, 1989.
12. E.W. Cheney, *Introduction to Approximation Theory*, Chelsea Pub. Co, New York, 1982.
13. D. Grosenick, H. Wabnitz, H.H. Rinneberg, K.T. Moesta and P.M. Schlag Development of a time-domain optical mammograph and first *in vivo* applications, *Applied Optics*, 38, 2827-2943, 1999
14. E. Isaacson and H.B. Keller, *Analysis of Numerical Methods*, Wiley, New York, 1966.

15. R. G. Novikov, Multidimensional inverse spectral problem for the equation $-\delta\psi + (v(x) - Eu(x))\psi = 0$, *Funk. Anal. Pril.* 22, 1122 (in Russian), 1988.
16. R. G. Novikov, The inverse scattering problem on a fixed energy level for the two-dimensional Schrodinger operator, *J. Funk. Anal.*, 103, 40963, 1992.
17. A. Nachman, Global uniqueness for a two-dimensional inverse boundary value problem, *Ann. Math.*, 143, 7196, 1996.
18. P.G. Grinevich, The scattering transform for the two-dimensional operator with a potential that decreases at infinity at fixed nonzero energy, *Russ. Math. Surv.*, 55, 370, 2000.
19. M.I. Belishev, Boundary control in reconstruction of manifolds and metrics (the BC method), *Inverse Problems*, 13, R145, 1997.
20. S.I. Kabanikhin, A.D. Satybaev and M.A. Shishlenin, *Direct Methods of Solving Multidimensional Inverse Hyperbolic Problems*, Utrecht: VSP, 2004.
21. V.A. Burov, S.A. Morozov and O.D. Rumyantseva, Reconstruction of fine-scale structure of acoustical scatterers on large-scale contrast background, *Acoust. Imaging*, 26, 2318, 2002.
22. S. Siltanen, J.L. Mueller and D. Isaacson, An implementation of the reconstruction algorithm of A. Nachman for the 2-D inverse conductivity problem, *Inverse Problems*, 16, 6819, 2000.
23. M.I. Belishev and V. Yu. Gotlib, Dynamical variant of the BC-method: theory and numerical testing, *J. Inverse Ill-Posed Problems*, 7, 22140, 1999.
24. M.V. Klibanov, A. Timonov, Numerical studies on the globally convergent convexification algorithm in 2D, *Inverse Problems*, 23, 123-138, 2007.

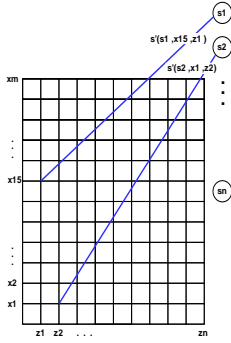


Figure 1. The figure illustrates construction of the real distance S in the asymptotic expansion of the tail function. The distance S measures the distance to any interior point individually, rather than the distance to the edge denoted by s .



Figure 2. These two figures illustrate the comparison of actual tail function $T(x, z, \bar{s})$ from forward problem (left panel) and the calculated tail function $T_1(x, z, \bar{s})$ derived from iterative procedure (right panel).

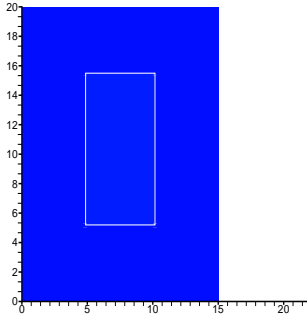


Figure 3. The figure illustrates relative positions of rectangles Ω_0 and Ω . The light source location is at the right edge Ω .

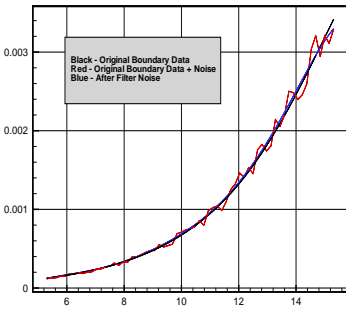
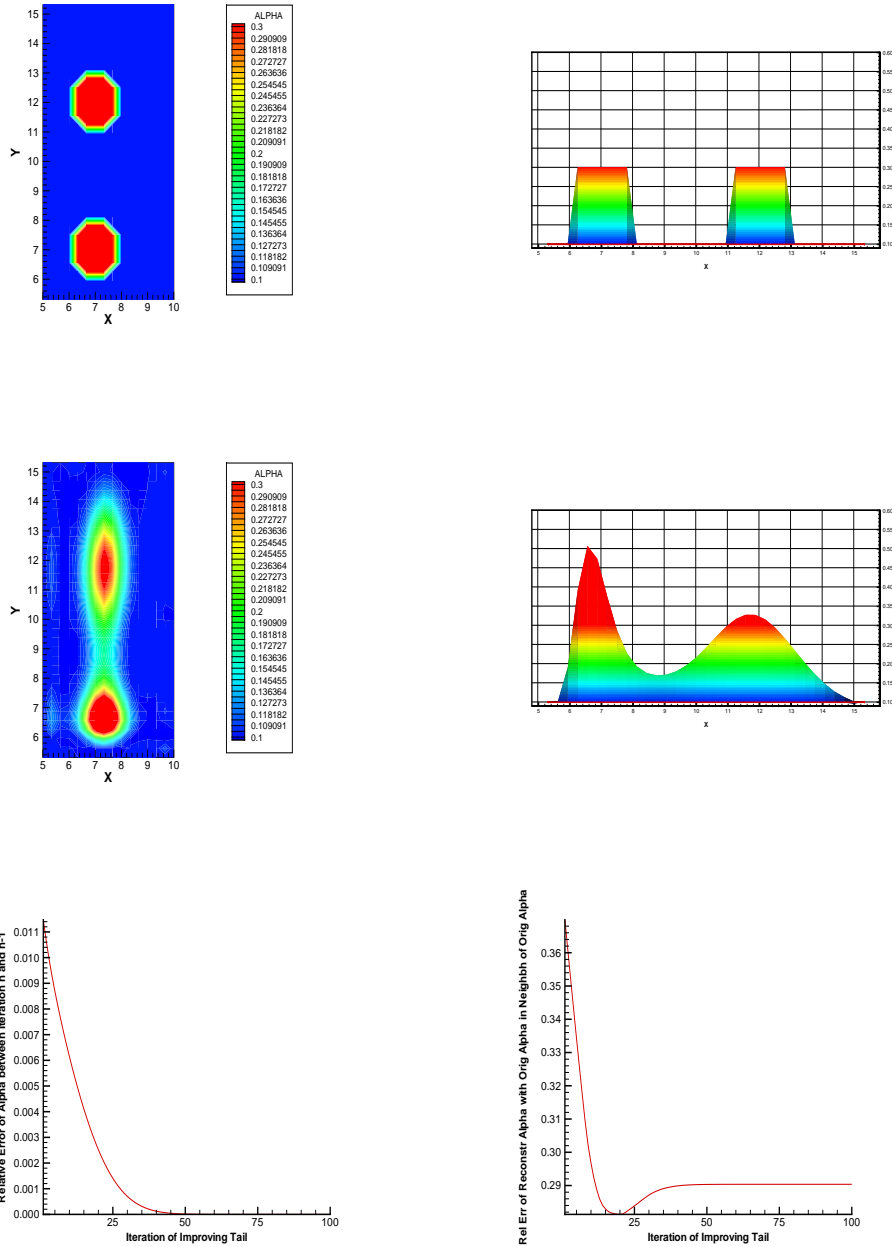


Figure 4. We use an eighth order polynomial to approximate functions $\tilde{\varphi}(x, s_k)$ and $\tilde{\psi}(x, s_k)$ with respect to x for each s_k . The polynomial is optimal in the least square sense, and its sub-routine is commonly available [11,12]. We demonstrate the essence of the approximation in Figure 4.



Figures 5a-5d. Figure 5a displays the original distribution. Figure 5b shows reconstruction from the noisy data. The 1-d cross sections next to the 2-d figures show the profiles of the original inclusion and its reconstruction at $z = 7$

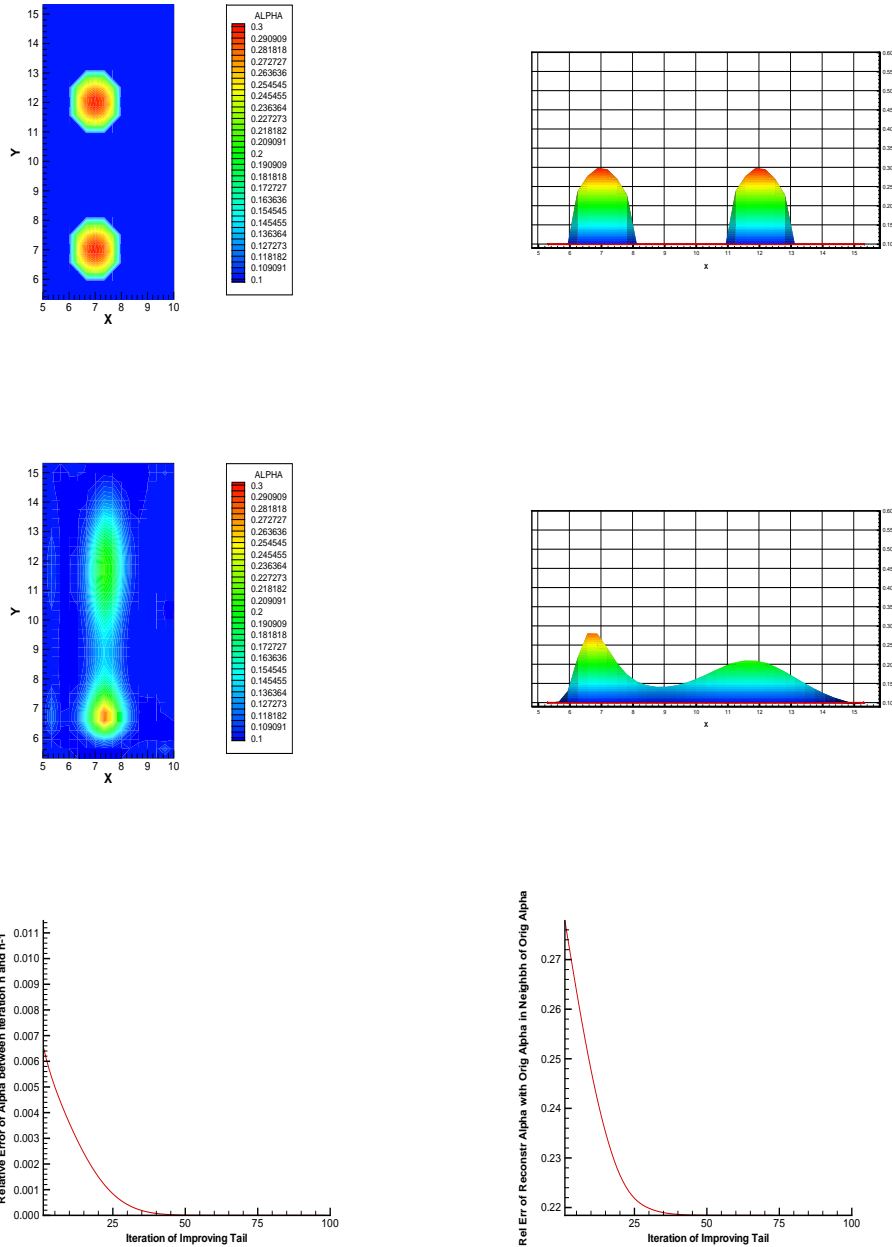
We illustrate on Figure 5c the difference of two consecutive reconstruction

$$||a_m(x, z) - a_{m-1}(x, z)|| \equiv \frac{\sqrt{\sum_{i=1, \dots, i_{max}, j=1, \dots, j_{max}} |(a_m(x_i, z_j) - a_{m-1}(x_i, z_j))|^2}}{\sqrt{N_1} \max |a_{m-1}(x_i, z_j)|}$$

as a function of the number of iteration m . The function is used for determining stopping criterion. Figure 5d depicts the relative error in comparison with actual inclusion expressed by

$$RMSE \equiv \frac{\sqrt{\sum_{i=1, \dots, i_{max}; j=1, \dots, j_{max}} |(a_m(x_i, z_j) - a(x_i, z_j))|^2}}{\sqrt{N_1} \max |a(x_i, z_j)|}$$

as a function of the number of iterations m .



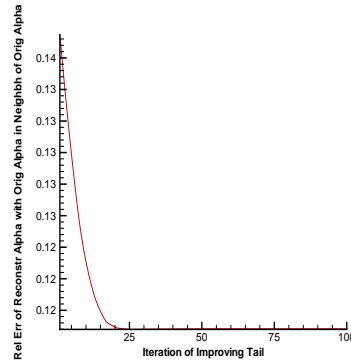
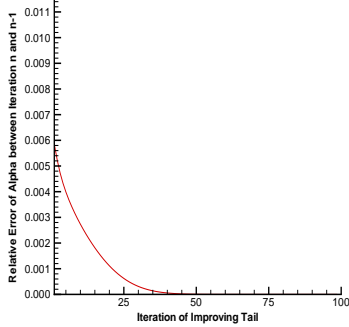
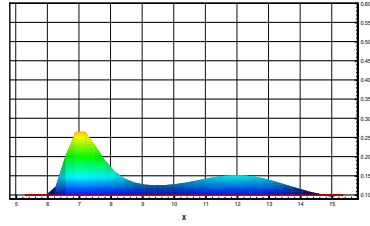
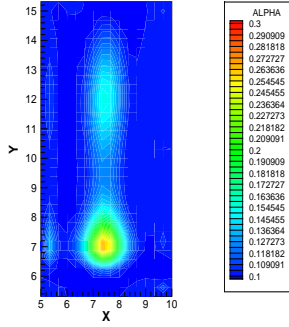
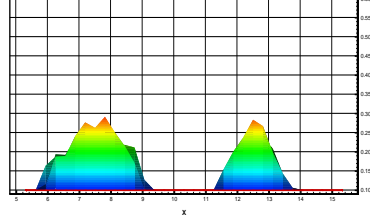
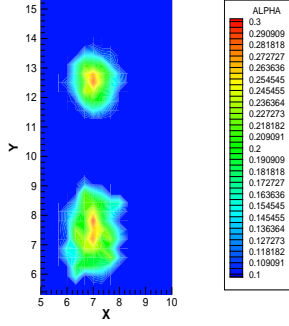
Figures 6a-6d. Figure 6a displays the original function in two inclusions. Figure 6b shows the reconstruction result with 2% noise. We illustrate on Figure 6c the difference of two consecutive reconstruction

$$||a_m(x, z) - a_{m-1}(x, z)|| \equiv \frac{\sqrt{\sum_{i=1, \dots, i_{max}; j=1, \dots, j_{max}} |(a_m(x_i, z_j) - a_{m-1}(x_i, z_j))|^2}}{\sqrt{N_1} \max |a_{m-1}(x_i, z_j)|}$$

as a function of the number of iteration m . The function is used for determining stopping criterion. Figure 6d depicts the relative error in comparison with actual inclusion expressed by

$$RMSE \equiv \frac{\sqrt{\sum_{i=1, \dots, i_{max}; j=1, \dots, j_{max}} |(a_m(x_i, z_j) - a(x_i, z_j))|^2}}{\sqrt{N_1} \max |a(x_i, z_j)|}$$

as a function of the number of iterations m .



Figures 7a-7d. Figure 6a displays the original distribution. Figure 7b displays the reconstruction result with 2% noise in the data. The 1-d cross sections show the profiles of the original inclusion and its reconstruction at $z = 7$. We illustrate on Figure 7c the difference of two consecutive reconstruction

$$\|a_m(x, z) - a_{m-1}(x, z)\| \equiv \frac{\sqrt{\sum_{i=1, \dots, i_{max}, j=1, \dots, j_{max}} |(a_m(x_i, z_j) - a_{m-1}(x_i, z_j))|^2}}{\sqrt{N_1} \max |a_{m-1}(x_i, z_j)|}$$

as a function of the number of iteration m . The function is used for determining stopping criterion. Figure 7d depicts the relative error in comparison with actual inclusion expressed by

$$RMSE \equiv \frac{\sqrt{\sum_{i=1, \dots, i_{max}; j=1, \dots, j_{max}} |(a_m(x_i, z_j) - a(x_i, z_j))|^2}}{\sqrt{N_1} \max |a(x_i, z_j)|}$$

as a function of the number of iterations m .